Spin Chern pumping from the bulk of two-dimensional topological insulators

M. N. Chen, L. Sheng, R. Shen, D. N. Sheng, and D. Y. Xing

Spin Chern Pumping from the Bulk of Two-Dimensional Topological Insulators

M. N. Chen[1], L. Sheng[1],*, R. Shen[1], D. N. Sheng[2], and D. Y. Xing[1]†

[1] *National Laboratory of Solid State Microstructures, Department of Physics,*
and Collaborative Innovation Center of Advanced Microstructures, Nanjing University, Nanjing 210093, China
[2] *Department of Physics and Astronomy, California State University, Northridge, California 91330, USA*

Topological insulators (TIs) are a new quantum state of matter discovered recently, which are characterized by unconventional bulk topological invariants. Proposals for practical applications of the TIs are mostly based upon their metallic surface or edge states. Here, we report the theoretical discovery of a bulk quantum pumping effect in a two-dimensional TI electrically modulated in adiabatic cycles. In each cycle, an amount of spin proportional to the sample width can be pumped into a nonmagnetic electrode, which is attributed to nonzero spin Chern numbers $C_\pm$. Moreover, by using a half-metallic electrode, universal quantized charge pumping conductivities $-C_\pm e^2/h$ can be measured. This discovery paves the way for direct investigation of the robust topological properties of the TIs.

I. INTRODUCTION

Topological transport phenomena have been attracting a great deal of interest, because they exhibit universal properties that are insensitive to perturbations and independent of material details. A classical example of such a transport phenomenon is the integer quantum Hall (IQH) effect in two-dimensional (2D) electron systems, first discovered in 1980,[1] which is characterized by an integer quantization of the Hall conductivity in unit of e^2/h. The IQH effect has been observed in a large variety of materials, ranging from traditional semiconductors, to oxides,[2] graphene,[3] and topological insulators (TIs).[4] Laughlin[5] interpreted the IQH effect in terms of an adiabatic charge pump. Thouless, Kohmoto, Nightingale, and Nijs[6] established a relation between the quantized Hall conductivity of the IQH system and a topological invariant, the first Chern number. Thouless and Niu[7,8] also related the amount of charge pumped in a 1D charge pump to the Chern number.

A variant of the IQH effect, the quantum spin Hall (QSH) effect, was proposed recently,[9,10] which has been experimentally realized in HgTe quantum wells[11] and InAs/GaSb bilayers.[12] Extension of the idea of the QSH effect has led to the discovery of 3D TIs.[13–16] A QSH system, which is also called a 2D TI, has an insulating band gap in the bulk and a pair of gapless helical edge states at the sample boundary. When the electron spin is conserved, a QSH system can be viewed as two independent IQH systems without Landau levels.[17] Different from the charge, the spin does not obey a fundamental conservation law. In general, when the spin conservation is absent, unconventional topological invariants, either the Z_2 index[18] or the spin Chern numbers,[19–21] are needed to describe the QSH systems. The time-reversal (TR) symmetry is considered to be a prerequisite for the QSH effect, which protects both the Z_2 index and gapless nature of the edge states. However, based upon the spin Chern numbers, it was shown that the bulk topological properties remain intact even when the TR symmetry is broken.[21] This finding evokes interest to pursue direct investigation and possibly utilization of the robust topological properties of the TIs, besides using their symmetry-protected gapless edge states which are more fragile in realistic environments.

Unlike the first Chern number underlying the IQH systems, which is embedded into the Hall conductivity, up to now the topological invariants in the TIs have not been directly observable. Several experimental methods were proposed, but have not been realized. One was to measure the topological magnetoelectric effect,[22,23] for which experimental complexities exist.[23] Fu and Kane[24] put forward an abstract 1D model, in which the spin pumping was related to the Z_2 index in the limit of weak coupling. However, how this fictitious model could be implemented is still unknown. Furthermore, from the viewpoint of application, generalization of the idea of the Z_2 pump to higher dimension is meaningless, because according to the Z_2 theory,[24] only the states at the TR-invariant point of the Brillouin zone can contribute to the spin pumping, and so the pumping rate cannot be enhanced by increment of dimension. In a recent work,[25] the more general case of finite coupling between the pump and electrode is investigated by using the scattering matrix method. It was found that the spin pumping in the model of Fu and Kane can survive finite scattering of magnetic impurities, and so may be attributed to the spin Chern numbers rather than the Z_2 index. Some other authors[26,27] proposed to pump quantized charge through the helical edge states by precessing a magnet covering the edge of a 2D TI, so that the number of gapless edge channels can be counted through electrical measurement. This method is indirect, in the sense that the topological invariants are intrinsic properties of the bulk electron wavefunctions, which do not immediately determine the charge pumping in the edge channels.

Here we predict an intriguing bulk topological pumping effect, directly driven by nonzero spin Chern numbers, in a QSH system electrically modulated in adiabatic cycles. As a consequence of the topological spectral flows of
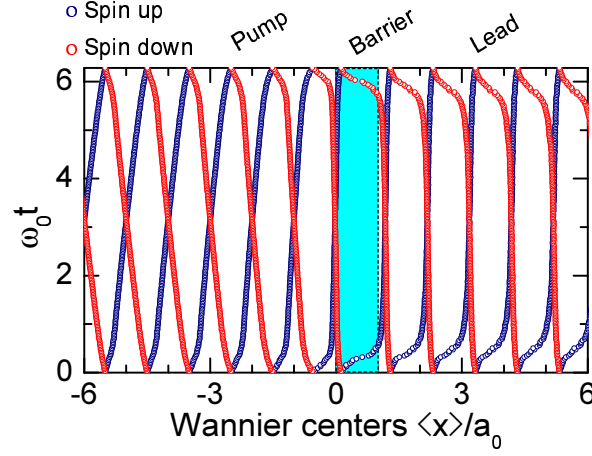
FIG. 1: Plot of the centers of mass of the SPWFs (horizontal axis) as functions of $\omega_0 t$ (vertical axis). The parameters are taken to be $k_y = 0.4 k_y^c$, $M_0 = v_F e A_0 = \hbar R_0 / a_0 = 0.1 t_0$, $V_0 = 0.3 t_0$, and $d = a_0$, with a_0 as the lattice constant and $t_0 = \hbar v_F / a_0$ ($v_F' = v_F$) as the hopping integral of the tight-binding Hamiltonian.

the spin-polarized Wannier functions (SPWFs) in the bulk of the system, spin can be pumped into a nonmagnetic electrode continuously without net charge transfer. The total amount of spin pumped per cycle is proportional to the (cross-section) width of the sample, and insensitive to the material parameters and spin-mixing effect due to the Rashba spin-orbit coupling. This electrical spin pump establishes a basis, on which spintronic applications taking advantage of the robust topological properties of the TIs can be developed. Especially, if a half-metallic electrode with spin polarization parallel (or antiparallel) to the z-axis is used, a quantized charge pumping conductivity, $-C_+ e^2 / h$ (or $-C_- e^2 / h$), can be measured by electrical means, demonstrating a way to observe the spin Chern numbers $C_\pm$ directly.

II. SPIN CHERN NUMBERS AND SPWFS

Let us consider a 2D model Hamiltonian $H_P = H_0 + H_1$ with

$$H_0 = v_F \left[k_x \hat{s}_z \hat{\sigma}_x - (k_y + e A(t)) \hat{\sigma}_y \right] - M(t) \hat{\sigma}_z . \tag{1}$$

Here $(-e)$ is the electron charge, $\mathbf{k}$ is the 2D momentum, $A(t) = A_0 \sin(\omega_0 t)$ is the vector potential of an *ac* electric field $-E_0 \cos(\omega_0 t)$ applied along the y direction with $A_0 = E_0 / \omega_0$ and frequency $\omega_0 > 0$ being designated, and $M(t) = M_0 \cos(\omega_0 t)$. This model can describe both the QSH materials, the HgTe quantum wells,[28–30] and InAs/GaSb bilayers,[31] in the linear order in momentum. For definity of discussion, we confine ourselves to the HgTe quantum wells, for which $\hat{s}_\alpha$ with $\alpha = x, y, z$ are the Pauli matrices for spin, and $\hat{\sigma}_\alpha$ for the electron and hole bands. As will be discussed below, the time-dependent mass term $M(t)$ can be induced by varying the voltages of the dual gates. H_1 represents the Rashba spin-orbit coupling[32]

$$H_1 = \frac{R_0}{2} (\hat{1} + \hat{\sigma}_z)[\hat{s}_y k_x - \hat{s}_x (k_y + e A(t))] . \tag{2}$$

To the linear order in momentum, the Rashba spin-orbit coupling is nonvanishing only in the electron band.[32]

Within the adiabatic approximation, for a bulk sample there exists a finite energy gap between the conduction and valence bands for $\omega_0 t \neq \pi/2$ or $3\pi/2$. At $\omega_0 t = \pi/2$ and $3\pi/2$, the conduction and valence bands touch at $k_x = 0$ and $k_y = k_y^c$ or $-k_y^c$ with $k_y^c = e|A_0| = e|E_0|/\omega_0$. To clarify the topological properties underlying the spin/charge pumping, we consider k_y as a parameter, and calculate the spin Chern numbers $C_\pm$ in the standard way,[21] on the torus of the two variables $k_x \in (-\infty, \infty)$ and $t \in [0, T)$ with $T = 2\pi/\omega_0$ as the period. The spin Chern numbers are obtained as

$$C_\pm = \pm \text{sgn}(E_0 M_0) , \tag{3}$$

for $|k_y| < k_y^c$, and vanish elsewhere. Not surprisingly, the band touching points $k_y = \pm k_y^c$ serve as the critical points.

We now consider a system consisting of a pump for $x < 0$, an electrode for $x > d$, and a potential barrier in between. The total Hamiltonian of the system reads

$$H = \begin{cases} H_P & (x < 0) \\ H_E + V_0\hat{\sigma}_z & (0 < x < d) \\ H_E & (x > d) \end{cases} \quad , \tag{4}$$

where H_P has been given above, and $H_E = v'_{\text{F}} k_x \hat{s}_z \hat{\sigma}_x$ is the Hamiltonian of the electrode. A possible experimental setup for realizing this Hamiltonian is explained in Appendix A in more details. In the barrier region, the term $V_0\hat{\sigma}_z$ opens an insulating gap of size $2V_0$, which accounts for contact deficiencies between the pump and electrode. The crucial role of the nonzero spin Chern numbers in the spin/charge pumping process can be visualized by using the SPWFs, which were first introduced in Ref.[25]. We construct a tight-binding Hamiltonian for the effective 1D system at any given k_y according to Eq. (4), and diagonalize the total Hamiltonian of the pump and electrode numerically. Following the same procedure as calculating the spin Chern numbers,[21] the space occupied by electrons is partitioned into two spin sectors after diagonalizing the spin operator $\hat{s}_z$ in the occupied space. By definition, the states in the two spin sectors are essentially the maximally spin-polarized states. Then we construct the Wannier functions[33,34] for the spin-up and spin-down sectors, respectively, which are called the SPWFs.

The evolution of the centers of mass of the SPWFs for $k_y = 0.4k_y^c$ and $R_0 = 0.1v_{\text{F}}$ is shown in Fig. 1. We see that the Wannier centers for the spin-up sector move right and those for the spin-down sector move left, each center shifting on average a lattice constant per cycle. Within the adiabatic approximation, time $t \in [0, T)$ plays the same role as the momentum of an additional dimension,[24] namely, $k_t \in [0, T)$. Therefore, when k_y is considered as a parameter, the evolution of the Wannier functions of the effectively 1D system related to various k_x with time t can be understood from the static properties of a 2D system associated with various k_x and k_t. In the general theory,[34] the relationship between the Chern number and the spectral flows of the Wannier functions in a 2D system has been established. According to this theory, the average displacement of each of the centers of the SPWFs in the spin-up (spin-down) sector with changing k_t (or t) from 0 to T, in units of the lattice constant, must equal to the spin Chern number $C_+ = 1$ ($C_- = -1$). Therefore, the nontrivial transfer of the SPWFs observed in Fig. 1 is a direct manifestation of the nonzero spin Chern numbers $C_\pm = \pm 1$ in the pump (for $E_0 M_0 > 0$). More interestingly, we see that such spectral flows can go across the finite barrier ($V_0 d > 0$), and extend into the electrode, even though the barrier and electrode are topologically trivial. Physically, because the system needs to recover its original eigenstates when each cycle ends, the nontrivial spectral flows of the SPWFs in the TI need to constitute closed loops through formation of edge states at the boundary,[35] or extend into the electrode. However, localized edge states can not exist at the finite barrier due to quantum tunneling effect, so the transfer of the spectral flows of the SPWFs into the electrode occurs. This result will be further confirmed by direct calculation based upon the scattering matrix theory in the next section.

The SPWFs are just another equivalent representation of the occupied space, and so the counter spectral flows of the Wannier centers in the two spin sectors represent the true movements of the electrons. If the Rashba spin-orbit coupling were neglected, the Wannier functions would be the eigenstates of $\hat{s}_z$. The nontrivial spectral flows indicate that at the given k_y, in each cycle a spin-up electron goes from the pump into the electrode, and a spin-down electron moves oppositely. Therefore, no net charge transfer occurs but a quantized spin of $2(\hbar/2)$ is pumped into the electrode. When the small Rashba spin-orbit coupling is turned on, while the topological spectral flows remain intact, as seen from Fig. 1, the spin polarizations of the Wannier functions are no longer fully parallel to the z-axis, and may also vary with time. As a consequence, the amount of spin pumped per cycle will deviate from the quantized value.

III. THE PROCESS OF SPIN CHERN PUMPING

A. Spin pumping for a nonmetallic electrode

In general, the amount of the spin pumped can be conveniently calculated by using the scattering matrix formula.[36,37] The z-component of the spin pumped per cycle is given by[36,37]

$$\Delta s_z(k_y) = \frac{\hbar}{4\pi i} \oint_T dt \left(r_{\uparrow\uparrow}^* \frac{dr_{\uparrow\uparrow}}{dt} - r_{\downarrow\downarrow}^* \frac{dr_{\downarrow\downarrow}}{dt} - r_{\downarrow\uparrow}^* \frac{dr_{\downarrow\uparrow}}{dt} + r_{\uparrow\downarrow}^* \frac{dr_{\uparrow\downarrow}}{dt} \right) , \tag{5}$$

where $r_{\alpha\beta}$ ($\alpha, \beta = \uparrow, \downarrow$) is the reflection amplitude for an electron at the Fermi energy incident from the spin-β channel of the electrode and reflecting back into the spin-α channel. In the following calculations, the Fermi energy is set to
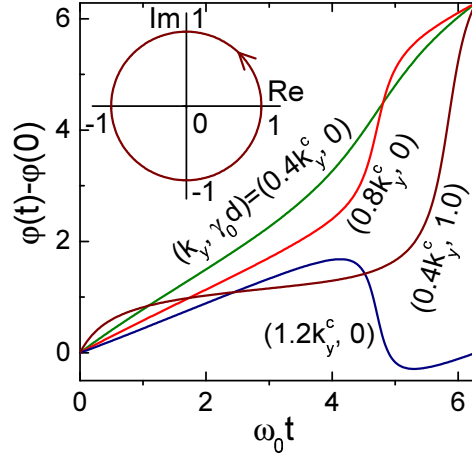
FIG. 2: Argument of the complex reflection amplitude, $\varphi(t) = \arg(r_{\uparrow\uparrow})$, as a function of $\omega_0 t$ for four sets of $(k_y, \gamma_0 d)$. The other parameters are taken to be $R_0 = 0$ and $v_F e A_0 = M_0$ with $k_y^c = e|A_0|$. Inset: trajectories of $r_{\uparrow\uparrow}$ in a cycle on the complex plane.

be zero ($E_F = 0$), and the Rashba spin-orbit coupling is treated as a perturbation. As shown in Appendix B, to the linear order in R_0, we obtain

$$r_{\uparrow\uparrow} = -\frac{\cos(2\theta) + i[\mathrm{sh}(2\gamma_0 d) - \sin(2\theta)\mathrm{ch}(2\gamma_0 d)]}{\mathrm{ch}(2\gamma_0 d) - \sin(2\theta)\mathrm{sh}(2\gamma_0 d)} + \mathcal{O}(\epsilon^2) , \tag{6}$$

$$r_{\downarrow\uparrow} = \frac{\epsilon}{2}\frac{\sin(2\theta)[1 - \cos(2\theta)]}{\mathrm{ch}(2\gamma_0 d) - \sin(2\theta)\mathrm{sh}(2\gamma_0 d)} + \mathcal{O}(\epsilon^2) , \tag{7}$$

and $r_{\downarrow\downarrow} = r_{\uparrow\uparrow}|_{2\theta \to (\pi - 2\theta)}$ and $r_{\uparrow\downarrow} = -r_{\downarrow\uparrow}|_{2\theta \to (\pi - 2\theta)}$, where $\gamma_0 = V_0/\hbar v_F'$ and $2\theta = \arg[v_F(k_y + eA(t)) + iM(t)]$. We note that the dimensionless quantity $\epsilon = R_0/v_F$ appears as the small expansion parameter. Since $r_{\downarrow\uparrow}$ and $r_{\uparrow\downarrow}$ are always real, the contributions from the third and fourth terms in Eq. (5) vanish. Consequently,

$$\Delta s_z(k_y) = \frac{\hbar}{4\pi i} \oint_T \left(r_{\uparrow\uparrow}^* dr_{\uparrow\uparrow} - r_{\downarrow\downarrow}^* dr_{\downarrow\downarrow}\right) . \tag{8}$$

This expression has a geometric explanation: the amount of spin pumped per cycle equals to the difference between the areas enclosed by the directional trajectories of $r_{\uparrow\uparrow}$ and $r_{\downarrow\downarrow}$ on the complex plane, multiplied by $\hbar/2\pi$. Due to the relation $r_{\downarrow\downarrow} = r_{\uparrow\uparrow}|_{2\theta \to (\pi - 2\theta)}$, yielding $r_{\downarrow\downarrow} = -\mathrm{Re}(r_{\uparrow\uparrow}) + i\mathrm{Im}(r_{\uparrow\uparrow})$, the two terms in Eq. (8) make an equal contribution, so that we can focus on the first term. While the expression (6) for $r_{\uparrow\uparrow}$ is independent of the Rashba spin-orbit coupling, as will be shown soon, a combination of Eqs. (6) and (7) allows us to evaluate the amount of spin pumped up to the second order in R_0/v_F.

We first consider the case of $R_0 = 0$. From Eq. (6), it is easy to show $|r_{\uparrow\uparrow}(k_y)| = 1$. In Fig. 2, we plot the argument $\varphi(t)$ of $r_{\uparrow\uparrow}(k_y)$ as a function of $\omega_0 t$ for several parameter sets. For either $\gamma_0 d = 0$ (ideal contact) or 1.0 (strong potential barrier), $\varphi(t)$ always increments 2π in a cycle as long as $|k_y| < k_y^c$. In this case, the trajectories of $r_{\uparrow\uparrow}(k_y)$ always form a unit circle on the complex plane, oriented counterclockwise, as shown in the inset of Fig. 2, suggesting $\Delta s_z(k_y) = \hbar$ (for $E_0 M_0 > 0$). For $|k_y| > k_y^c$, however, the situation is quite different. $\varphi(t)$ does not change after going through a cycle, and the trajectory of $r_{\uparrow\uparrow}(k_y)$ does not enclose a finite area, so that $\Delta s_z(k_y) = 0$. Apparently, the present result conforms to the spin Chern numbers given by Eq. (3) and the spectral flows of the SPWFs.

Next we study the correction to $\Delta s_z(k_y)$ due to nonzero Rashba spin-orbit coupling. By expressing $r_{\uparrow\uparrow} = \rho e^{i\varphi} = \sqrt{1 - \delta\rho^2} e^{i(\varphi^{(0)} + \delta\varphi)}$ in the polar coordinate system, where $\varphi^{(0)}$ is the argument at $R_0 = 0$, and $\delta\varphi$ and $\delta\rho^2$ stand for the second-order corrections to φ and ρ^2, respectively, due to the Rashba spin-orbit coupling, Eq. (8) becomes $\Delta s_z(k_y) = (\hbar/2\pi)[\oint_T (1 - \delta\rho^2)d\varphi^{(0)} + \oint_T d\delta\varphi] + \mathcal{O}(\epsilon^3)$. We notice that $\delta\varphi$ is a small quantity fluctuating around 0 and periodic in time, $\delta\varphi|_{t=0} = \delta\varphi|_{t=T}$, so that $\oint_T d\delta\varphi = 0$. Using the identity $\delta\rho^2 = |r_{\downarrow\uparrow}|^2$, we then obtain $\Delta s_z(k_y) = (\hbar/2\pi)\oint_T (1 - |r_{\downarrow\uparrow}|^2)d\varphi^{(0)}$, where $d\varphi^{(0)}$ can be calculated from Eq. (6) and $r_{\downarrow\uparrow}$ has been given by Eq. (B26). This is an expression for $\Delta s_z(k_y)$ accurate to the second order in R_0/v_F. At $\gamma_0 d = 0$, we obtain $\Delta s_z(k_y)$ as

$$\Delta s_z(k_y) \simeq \frac{\hbar}{2}\left[1 - \frac{5}{32}\left(\frac{R_0}{v_F}\right)^2\right](C_+ - C_-) , \tag{9}$$
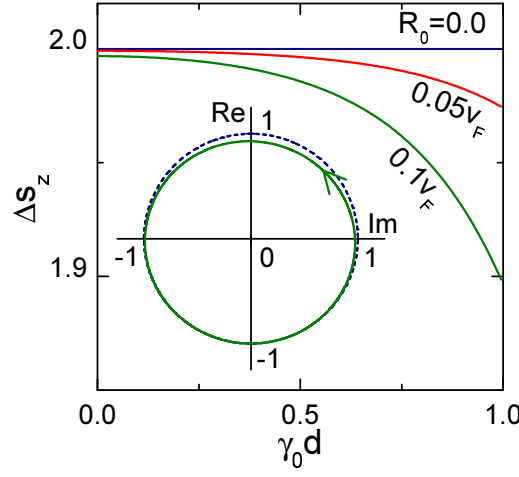
FIG. 3: $\Delta s_z(k_y)$ (in unit of $\hbar/2$) as a function of $\gamma_0 d$ for $k_y = 0.4k_y^c$ and three different values of R_0. The other parameters are taken to be the same as in Fig. 2. Inset: the trajectory of $r_{\uparrow\uparrow}$ in a cycle for $R_0 = 0.1v_{\mathrm{F}}$ and $\gamma_0 d = 1.0$, with the unit circle indicated by the dotted line.

for $|k_y| < k_y^c$, and $\Delta s_z(k_y) = 0$ elsewhere. As expected, nonzero Rashba spin-orbit coupling causes $\Delta s_z(k_y)$ to deviate from its quantized value, i.e., $(C_+ - C_-)\hbar/2$. In real materials, R_0 is usually much smaller (by an order of magnitude or more) than v_{F},[32] so that the deviation is less than a percent for an ideal connection between the pump and electrode.

For $\gamma_0 d \neq 0$, $\Delta s_z(k_y)$ can be evaluated numerically and its calculated result is plotted in Fig. 3 as a function of $\gamma_0 d$ for three different strengths of the Rashba spin-orbit coupling. For $R_0 = 0$, $\Delta s_z(k_y)$ is quantized to $\hbar$, independent of $\gamma_0 d$. For $R_0 = 0.05v_{\mathrm{F}}$ and $0.1v_{\mathrm{F}}$, weak potential barrier ($\gamma_0 d \ll 1$) has little effect on $\Delta s_z(k_y)$. This is reasonable as the leading-order correction of small $\gamma_0 d$ must be $\mathcal{O}(\epsilon^2 \gamma_0 d)$. Appreciable deviations from the quantized value occur for strong potential barrier (e.g., $\gamma_0 d \simeq 1$). We note that $\delta\varphi$ does not affect the orbit of $r_{\uparrow\uparrow}$, as it represents a variation in the tangent direction of the orbit, and the orbit can be determined by $r_{\uparrow\uparrow} = \sqrt{1 - |r_{\downarrow\uparrow}|^2}e^{i\varphi^{(0)}}$. Inset shows the trajectory of $r_{\uparrow\uparrow}$ on the complex plane for $R_0 = 0.1v_{\mathrm{F}}$ and $\gamma_0 d = 1.0$. For such a strong potential barrier, the orbit of $r_{\uparrow\uparrow}$ deviates from the unit circle visibly. The above result suggests that improving the contact quality between the pump and electrode is helpful for obtaining a nearly integer-quantized value of the pumped spin.

By summing over k_y between $-k_y^c$ and k_y^c, we obtain for the total spin pumped per cycle

$$\Delta S_z = \sigma_s(2|E_0|L_y/\omega_0) , \tag{10}$$

with

$$\sigma_s \simeq \frac{e}{4\pi}\left[1 - \frac{5}{32}\left(\frac{R_0}{v_{\mathrm{F}}}\right)^2\right](C_+ - C_-) , \tag{11}$$

for a good contact ($\gamma_0 d \ll 1$). ΔS_z is in scale with width L_y of the pump. By noting that ω_0 is proportional to the number of cycles per unit time, σ_s can be considered as the spin pumping conductivity.

B. Charge pumping for a half-metallic electrode

Now we discuss a possible way to experimentally observe the spin Chern numbers, by using a half-metallic electrode, in which conducting channels for electron spin antiparallel to the spin polarization are absent. We first consider the case, where the spin polarization of the electrode is parallel to the z axis. The Hamiltonian of the electrode is taken as $H_E = v'_{\mathrm{F}}(k_y)k_x\hat{s}_z\hat{\sigma}_x + V_1(\hat{1} - \hat{s}_z)\hat{\sigma}_z/2$. In this case, as shown in Appendix C, $r_{\uparrow\uparrow}$ is still given by Eq. (6) but $r_{\downarrow\uparrow} \equiv 0$. It follows that for any k_y between $-k_y^c$ and k_y^c, the charge pumped per cycle is integer-quantized and equal to $\Delta q(k_y) = (-e)C_+$. Similarly, for the spin polarization of the electrode antiparallel to the z axis, the charge pumped is equal to $\Delta q(k_y) = (-e)C_-$. Therefore, the total charge pumped per cycle is given by

$$\Delta Q = \sigma_c(2|E_0|L_y/\omega_0) , \tag{12}$$

with

$$\sigma_c = -C_\pm\frac{e^2}{h} , \tag{13}$$

where the spin Chern number C_+ (C_-) is taken for the spin polarization of the electrode parallel (antiparallel) to the z axis. We emphasize that Eqs. (12) and (13) obtained above are valid for finite Rashba spin-orbit coupling and finite potential barrier between the pump and electrode, indicating that the quantized charge pumping is robust against small perturbations. Experimentally, ΔQ can be obtained by measuring the electrical current in the electrode, and from Eqs. (12) and (13), $C_\pm$ can be evaluated, yielding an experimental method to measure the spin Chern numbers directly. The sign inversion of ΔQ with reversing the spin polarization of the half-metallic electrode, as indicated by Eqs. (12) and (13), is a hallmark of the present spin Chern charge pump, which can be used to distinguish it from the conventional Thouless charge pump[7,8].

We have used the single-electron approximation, where the electron interaction is not taken into account. In particular, in the half-metallic electrode case, one of the spin channel is blocked at the boundary, which naturally induces some charge and spin accumulations, and consequently changes the potential profile. However, owing to the screening effect, the change in the potential profile is expected to be localized at the boundary, which in effect modifies the potential barrier between the pump body and the electrode. As has been shown above, the charge pumping effect is independent of the existence and details of the potential barrier, and so we believe that the pumping effect will survive the charge and spin accumulations.

IV. DISCUSSION

Up to now, all the results obtained from the scattering matrix formula are apparently in complete agreement with the spin Chern numbers given by Eq. (3). These results cannot be explained within the framework of the Z_2 theory.[24] While one can define a Z_2 index at the TR-invariant point $k_y = 0$, the effective 1D Hamiltonian given by Eqs. (1) and (2) for any given nonzero k_y does not preserve the TR symmetry, as its TR partner is at $-k_y$, making the Z_2 index invalid. The Z_2 theory predicted that the TR symmetry is crucial for the topological spin pumping,[24] suggesting that only the states at the TR-invariant point $k_y = 0$ can contribute to the spin pumping. This clearly contradicts the present result that all the states with $|k_y| < k_y^c$ contribute equally, which is obtained directly from the scattering matrix formula. This point is also evidenced by the fact that the total amount of charge or spin pumped per cycle is in proportion to the sample width L_y. For the same reason, the pumping effect found in this work is also essentially different from that via edge states in Refs.[26,27], where the amount of spin or charge pumped per cycle is proportional to the number of the gapless edge channels.

In conclusion, our work uncovers a bulk topological pumping effect due to direct transfer of the SPWFs between the pump and electrode, without the participation of edge states. This measurable effect reveals the bulk topological properties of the system that are neither captured by the Z_2 index nor reflected by the number of gapless edge channels. It can be accurately described by the spin Chern numbers. This spin Chern pump may lay the foundation for direct experimental study and possibly utilization of the robust topological properties of the TIs.

The previous experimental work[38] evidenced the difficulty of modulating in time the properties of an open quantum dot without generating undesired bias voltages due to stray capacitances. This problem might not be significant in our pumping setup, where a much larger bulk sample of the TI can be used and the stray capacitances can be greatly reduced. Moreover, a possible way around the obstacle is to use the ac Josephson effect to induce periodically time-dependent Andreev reflection amplitudes in a hybrid normal-superconducting system.[39] Concrete design of a spin Chern pump based upon the Josephson effect will await future work. While the proposed spin pumping scheme may have the advantage of low noises, its practical application in spintronic devices still relies on the discovery of new TIs with bulk band gaps much greater than room temperature, which determine the temperature range where the spin Chern pumping effect can survive. Currently, precessing magnetization is a feasible method to generate robust spin currents in spintronic devices at room temperature.[40]
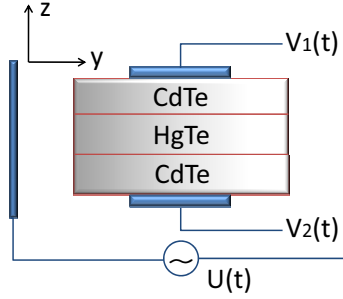
FIG. 4: A schematic view of a experimental setup for realization of a 2D spin Chern pump. A CdTe/HgTe/CdTe quantum well heterostructure, with dual gates on its top and bottom, is placed between two conductive plates. When the voltages of the gates and plates are adiabatically modulated in proper cycles, spin or charge can be pumped into electrodes coupled to the quantum well along the x direction.

Appendix A: A POSSIBLE EXPERIMENTAL REALIZATION OF THE SPIN CHERN PUMP

In what follows we expand on the model setup and possible experimental realization of the spin Chern pump in more details.

1. The pump

A possible experimental realization of the Hamiltonian Eq. (1) for the pump is illustrated in Fig. 4. A HgTe/CdTe quantum-well heterostructure with dual gates (top and bottom) is placed between two conductive plates. It is known that when the width of the quantum well (thickness of the HgTe film) is above a critical size $d_c = 6.3nm$,[28,29] the band structure is inverted, characterized a negative mass term $-M_0\hat{\sigma}_z$ in the Hamiltonian, corresponding to the QSH state. If the width of the quantum well falls below d_c, the band structure will be aligned in a "normal" way with a positive mass term $M_0\hat{\sigma}_z$, corresponding to a normal insulator. As has been discussed in Refs.[30] and[31], the topological phase transition between the QSH phase and normal insulator can also be tuned by applying a gate voltage, which effectively reduces the width of the quantum well. It is assumed that the quantum well under consideration has a width somewhat greater than d_c, and so has a negative mass term $-M_0\hat{\sigma}_z$ initially. With increasing the gate voltage, the electron mass increases, and can invert its sign. Usually, increasing the gate voltage may also adjust the carrier density. Nevertheless, it has been shown[30,31] that, by using dual gates and properly tuning their voltages $V_1(t)$ and $V_2(t)$, it is generally possible to change the electron mass in the desired manner to be $-M_0\cos(\omega_0 t)$, while keeping the electron Fermi energy still in the band gap.

The effect of the conductive plates is easily understood. When a voltage drop $U(t)$ is applied across the plates, a uniform electric field $\mathbf{E}(t) = E(t)\hat{\mathbf{y}}$ will be generated in the space between the two plates. The electrons in the quantum well experience a vector potential $\mathbf{A}(t) = A(t)\hat{\mathbf{y}}$ with $A(t)$ defined as $E(t) = -\partial A(t)/\partial t$. If the electric field is chosen to be $E(t) = -E_0\cos(\omega_0 t)$, one gets $A(t) = A_0\sin(\omega_0 t)$ with $A_0 = E_0/\omega_0$, as desired. We point out that the exact time dependencies of $M(t)$ and $A(t)$ are not essential for realizing the spin Chern pump, provided that they have the same periodicity and a constant relative phase shift.

2. The nonmagnetic electrode

The pumping effect is insensitive to material details of the electrode. The electrode is taken to be a normal metal with a 2D parabolic Hamiltonian $H_E = -E_0 + p^2/2m$. When E_0 is sufficiently large, for a given p_y, we can linearize the effective 1D Hamiltonian H_E at the right and left Fermi points $p_x = \pm mv'_F(k_y)$ with $v'_F(k_y) = \sqrt{2m(E_F + E_0) - k_y^2}/m$. A Pauli matrix $\hat{\sigma}_x$ is introduced to describe the two branches. To be consistent with the form of the Hamiltonian in the pump, we use $\sigma_x = 1$ and -1, respectively, to represent the right-moving and left-moving branches for $s_z = 1$ and oppositely for $s_z = -1$. As a result, the Hamiltonian of the electrode becomes $H_E = v'_F(k_y)k_x\hat{s}_z\hat{\sigma}_x$ at $E_F = 0$, where $k_y = p_y$ and $k_x = p_x \mp mv'_F(k_y)$. The spin pumping effect is usually dominated by small k_y, so that we can further approximate $v'_F(k_y) \simeq v'_F(k_y = 0) \equiv v'_F$, with purpose to minimize the number of adjustable parameters in the model.

3. The barrier

For the present Dirac-like Hamiltonian, an ordinary potential barrier has a very weak effect on the electron transmission due to the Klein paradox. Therefore, we take the Hamiltonian for the barrier to be $H_B = H_E + V_0\hat{\sigma}_z$. The inclusion of potential $V_0\hat{\sigma}_z$ opens up an insulating energy gap of size $2V_0$ around the Fermi level, which presumably is more efficient for describing the contact deficiencies and structural mismatch between the pump and electrode.

4. The half-metallic electrode

The half metal, e.g., CrO_2, $La_{2/3}Sr_{1/3}MnO_3$, etc., is a substance that acts as a conductor to electrons of one spin orientation, but as an insulator to those of the other spin orientation. From the viewpoint of the electronic structure, one of the spin subbands is metallic, whereas the Fermi level falls into an energy gap of the other spin subband. To simulate the half-metallic electrode, H_E is taken to be $H_E = v'_{\rm F}(k_y)k_x\hat{s}_z\hat{\sigma}_x + V_1(\hat{1} \mp \hat{s}_z)\hat{\sigma}_z/2$, where $\mp$ stands for the spin polarization of the electrode parallel and antiparallel to the z-axis, respectively. The second term opens an energy gap of size $2V_1$ around the Fermi level for electron spin antiparallel to the spin polarization of the electrode, without affecting the other spin subband. As a result, the electron density of states is fully spin-polarized at the Fermi energy. V_1 is set to be infinity in the final result.

Appendix B: CALCULATION OF THE REFLECTION AMPLITUDES FOR A NONMAGNETIC ELECTRODE

1. Electron wavefunctions in the pump and potential barrier

We now solve the scattering problem for an electron at the Fermi energy incident from the electrode. The Fermi energy will be taken to be $E_{\rm F} = 0$, which is in the band gap of the pump. Therefore, the incident electron will be fully reflected back into the electrode. The Rashba spin-orbit coupling is treated as a perturbation, and the result will be calculated to the linear order in the small quantity $\epsilon = R_0/v_{\rm F}$. The wavefunctions of the pump ($x < 0$), barrier ($0 < x < d$) and electrode ($x > d$) are denoted by $\Psi_P(x)$, $\Psi_B(x)$, and $\Psi_E(x)$, respectively. We have two boundary conditions: $\Psi_P(0^-) = \Psi_B(0^+)$ and $\Psi_B(d - 0^+) = \Psi_E(d + 0^+)$.

We use $\uparrow$ and $\downarrow$ to represent the eigenstates of $\hat{s}_z$, and $+1$ and -1 to represent those of $\hat{\sigma}_z$. On the basis $|\uparrow, +1\rangle$, $|\uparrow, -1\rangle$, $|\downarrow, +1\rangle$, and $|\downarrow, -1\rangle$, the Hamiltonian of pump (the Eqs. (1) and (2) in the manuscript) can be expanded as a 4×4 matrix

$$H_P = \begin{pmatrix} -M(t) & v_{\rm F}(k_x + i\tilde{k}_y) & R_0(-ik_x - \tilde{k}_y) & 0 \\ v_{\rm F}(k_x - i\tilde{k}_y) & M(t) & 0 & 0 \\ R_0(ik_x - \tilde{k}_y) & 0 & -M(t) & v_{\rm F}(-k_x + i\tilde{k}_y) \\ 0 & 0 & v_{\rm F}(-k_x - i\tilde{k}_y) & M(t) \end{pmatrix} \tag{B1}$$

where $\tilde{k}_y = k_y + eA(t)$. For energy $E = E_{\rm F} = 0$, the eigen-equation is obtained from Eq. (B1)

$$[M^2(t) + v_{\rm F}^2\tilde{k}^2]^2 - M^2(t)R_0^2\tilde{k}^2 = 0 , \tag{B2}$$

with $\tilde{k}^2 = k_x^2 + \tilde{k}_y^2$, and up to a normalization factor, the eigenfunctions are

$$\begin{pmatrix} A_1M(t)/v_{\rm F} \\ -A_1(k_x - i\tilde{k}_y) \\ A_2M(t)/v_{\rm F} \\ A_2(k_x + i\tilde{k}_y) \end{pmatrix} e^{ik_x x/\hbar} , \tag{B3}$$

where $A_1 = -(ik_x + \tilde{k}_y)M(t)$ and $A_2 = [M^2(t) + v_{\rm F}^2\tilde{k}^2]/R_0$. We need to solve k_x from the eigen-equation Eq. (B2). We notice that the equation is a 4th-degree polynomial of k_x with real coefficients, so complex conjugate roots must appear in pairs. Moreover, Eq. (B2) is even in k_x, so positive and negative roots appear in pairs. In combination, Eq. (B2) must have four roots of the form $k_x = a + ib$, $a - ib$, $-a + ib$, and $-a - ib$. By substitution of the four roots into Eq. (B3), we can in principle obtain four different eigenfunctions. For the present scattering problem, we only need the two eigenfunctions that are decaying into the pump, which correspond to the two roots with negative imaginary parts.

For $R_0 = 0$, it is easy to obtain for the roots for the two decaying modes: $k_x = -i\hbar\eta$ with $\hbar\eta = \sqrt{M^2(t) + \tilde{k}_y^2}$, which are two-fold degenerate. The corresponding two decaying eigenfunctions are given by

$$\varphi_+(x) = |\uparrow\rangle \otimes \begin{pmatrix} \sin\theta \\ i\cos\theta \end{pmatrix} e^{\eta x} , \tag{B4}$$

$$\varphi_-(x) = |\downarrow\rangle \otimes \begin{pmatrix} \cos\theta \\ -i\sin\theta \end{pmatrix} e^{\eta x} , \tag{B5}$$

where $2\theta = \mathrm{Arg}[v_\mathrm{F}\tilde{k}_y + iM(t)]$. For $R_0 \neq 0$, we write the roots of k_x as $k_x = -i\hbar\eta + \delta k_x$, and also write k_x^2 as $k_x^2 = -(\hbar\eta)^2 + \delta k_x^2$. To the second order in ϵ, we can solve for δk_x^2 from the eigen-equation Eq. (B2)

$$\delta k_x^2 = \left(\pm i\frac{R_0}{v_\mathrm{F}} + \frac{R_0^2}{2v_\mathrm{F}^2}\right)(\hbar\eta)^2 \sin^2(2\theta) + \mathcal{O}(\epsilon^3) . \tag{B6}$$

Noticing that the expression for A_2 given below Eq. (B3) has a factor R_0 in the denominator, we keep δk_x^2 to the second order, for the purpose to calculate A_2 to the linear order. By using the relation $\delta k_x^2 = -2i\hbar\eta\delta k_x + \mathcal{O}(\epsilon^2)$, we derive from Eq. (B6)

$$\delta k_x = \mp\frac{R_0}{2v_\mathrm{F}}\hbar\eta\sin^2(2\theta) + \mathcal{O}(\epsilon^2) . \tag{B7}$$

With these relations, we obtain for A_1 and A_2

$$A_1 = -v_\mathrm{F}(\hbar\eta)^2\sin(2\theta)[1 + \cos(2\theta)] \tag{B8}$$

$$\pm \ i\frac{R_0}{2}(\hbar\eta)^2\sin^3(2\theta) + \mathcal{O}(\epsilon^2) , \tag{B9}$$

and

$$A_2 = \left(\pm i + \frac{R_0}{2v_\mathrm{F}}\right)v_\mathrm{F}(\hbar\eta)^2\sin^2(2\theta) + \mathcal{O}(\epsilon^2) . \tag{B10}$$

We can always eliminate any common factor that appears in all the four components of Eq. (B3), whenever possible. By eliminating a common factor $2v_\mathrm{F}(\hbar\eta)^2\sin(2\theta)\cos\theta$, we rewrite A_1 and A_2 as

$$A_1 = -\cos\theta \pm i\frac{R_0}{2v_\mathrm{F}}\sin\theta\sin(2\theta) + \mathcal{O}(\epsilon^2) , \tag{B11}$$

and

$$A_2 = \left(\pm i + \frac{R_0}{2v_\mathrm{F}}\right)\sin\theta + \mathcal{O}(\epsilon^2) . \tag{B12}$$

Then the two decaying wavefunctions can be derived to be

$$\varphi_{1,2}(x) = \begin{pmatrix} -\cos^2\theta\sin\theta\left(1 \mp i\frac{R_0}{v_\mathrm{F}}\sin^2\theta\right) \\ -i\cos^3\theta\left(1 \mp 2i\frac{R_0}{v_\mathrm{F}}\sin^2\theta\right) \\ \pm i\sin^2\theta\cos\theta\left(1 \mp i\frac{R_0}{2v_\mathrm{F}}\right) \\ \pm\sin^3\theta\left[1 \mp i\left(\frac{1}{2} + \cos^2\theta\right)\frac{R_0}{v_\mathrm{F}}\right] \end{pmatrix} e^{\eta_\mp x} , \tag{B13}$$

where $\eta_\mp = \eta\left[1 \mp \frac{R_0}{2v_\mathrm{F}}\sin^2(2\theta)\right]$.

Some remarks are in order. With respect to the wavefunctions at $R_0 = 0$, namely, Eqs. (B4) and (B5), nonzero R_0 leads to nonperturbative change in the wavefunctions Eq. (B13), in the sense that Eq. (B13) will not recover Eqs. (B4) and (B5) in the limit $R_0 \to 0$. This is reasonable, just as what always happens in the degenerate perturbation theory of the quantum mechanics. For the present problem, the wavefunction $\Psi_P(x)$ in the pump is always expressed as an arbitrary linear superposition of the two decaying modes: $\Psi_P(x) = B_1\varphi_1(x) + B_2\varphi_2(x)$. By defining $\varphi_+(x) = -[\varphi_1(x) + \varphi_2(x)]$ and $\varphi_-(x) = -i[\varphi_1(x) - \varphi_2(x)]$, we can rewrite $\Psi_P(x)$ as $\Psi_P(x) = D_1\varphi_+(x) + D_2\varphi_-(x)$. The

final result for the reflection amplitudes depends only on $\Psi_P(x = 0^-)$, so we explicitly write out the expression for $\Psi_P(x = 0^-)$ as follows

$$\Psi_P(x = 0^-) = D_1\varphi_+(0^-) + D_2\varphi_-(0^-) , \tag{B14}$$

where

$$\varphi_+(0^-) = \begin{pmatrix} \sin\theta \\ i\cos\theta \\ -\frac{\sin^2\theta}{\cos^2\theta}\cos\theta\frac{R_0}{2v_F} \\ i\left(\frac{1}{2} + \cos^2\theta\right)\frac{\sin^3\theta}{\cos^2\theta}\frac{R_0}{v_F} \end{pmatrix} , \tag{B15}$$

$$\varphi_-(0^-) = \begin{pmatrix} \cos^2\theta\sin\theta\frac{R_0}{v_F} \\ 2i\cos^3\theta\frac{R_0}{v_F} \\ \cos\theta \\ -i\sin\theta \end{pmatrix} \tag{B16}$$

Now we see that in the limit $R_0 \to 0$, the total wavefunction $\Psi_P(0^-)$ will go back to the form of a superposition of the two decaying wavefunctions given in Eqs. (B4) and (B5). In conclusion, while small Rashba spin-orbit coupling may cause a nonperturbative change of the individual decaying wavefunctions, it modifies the "space" spanned by the two decaying modes in a perturbative manner. It is this "space" which determines the final result of the reflection amplitudes. This is the physical reason why in the final result, the Rashba spin-orbit coupling modifies the reflection amplitudes in a perturbative manner. The wavefunction in the potential barrier can be written as

$$\Psi_B(x) = \frac{C_1}{\sqrt{2}}|\uparrow\rangle \otimes \begin{pmatrix} 1 \\ -i \end{pmatrix} e^{\gamma_0 x} + \frac{C_2}{\sqrt{2}}|\uparrow\rangle \otimes \begin{pmatrix} 1 \\ i \end{pmatrix} e^{-\gamma_0 x} + \frac{C_3}{\sqrt{2}}|\downarrow\rangle \otimes \begin{pmatrix} 1 \\ i \end{pmatrix} e^{\gamma_0 x} + \frac{C_4}{\sqrt{2}}|\downarrow\rangle \otimes \begin{pmatrix} 1 \\ -i \end{pmatrix} e^{-\gamma_0 x} , \tag{B17}$$

where $\gamma_0 = V_0/\hbar v_F'$.

2. An electron incident from the spin-up channel

For an electron incident from the spin-up channel, the wavefunction in the electrode is given by

$$\begin{aligned} \Psi_E(x) &= \frac{1}{\sqrt{2}}|\uparrow\rangle \otimes \begin{pmatrix} 1 \\ -1 \end{pmatrix} + \frac{r_{\uparrow\uparrow}}{\sqrt{2}}|\uparrow\rangle \otimes \begin{pmatrix} 1 \\ 1 \end{pmatrix} \\ &+ \frac{r_{\downarrow\uparrow}}{\sqrt{2}}|\downarrow\rangle \otimes \begin{pmatrix} 1 \\ -1 \end{pmatrix} . \end{aligned} \tag{B18}$$

First, matching the wavefunctions Eqs. (B17) and (B18) at $x = d$, one obtain

$$C_1 = \frac{1}{2}[(1 - i) + r_{\uparrow\uparrow}(1 + i)]e^{-\gamma_0 d} , \tag{B19}$$

$$C_2 = \frac{1}{2}[(1 + i) + r_{\uparrow\uparrow}(1 - i)]e^{\gamma_0 d} , \tag{B20}$$

$$C_3 = \frac{r_{\downarrow\uparrow}}{2}(1 + i)e^{-\gamma_0 d} , \tag{B21}$$

$$C_4 = \frac{r_{\downarrow\uparrow}}{2}(1 - i)e^{\gamma_0 d} . \tag{B22}$$

In the next step, we will match wavefunctions at $x = 0$. Substituting Eqs. (B19-B22) into Eq. (B17), we can write Eq. (B17) at $x = 0^+$ as

$$\Psi_B(0^+) = \frac{1}{\sqrt{2}} \begin{pmatrix} \Gamma_+(2\gamma_0 d) + r_{\uparrow\uparrow}\Gamma_-(2\gamma_0 d) \\ -\Gamma_-(2\gamma_0 d) + r_{\uparrow\uparrow}\Gamma_+(2\gamma_0 d) \\ r_{\downarrow\uparrow}\Gamma_-(2\gamma_0 d) \\ -r_{\downarrow\uparrow}\Gamma_+(2\gamma_0 d) \end{pmatrix} \tag{B23}$$

where $\Gamma(\xi) = \mathrm{ch}(\xi) \pm i\mathrm{sh}(\xi)$. Now equating Eq. (B14) with Eq. (B23), we obtain

$$
\begin{pmatrix} i\sin^2\theta & \sin\theta\cos\theta \\ -\sin\theta\cos\theta & i\cos^2\theta \end{pmatrix} \begin{pmatrix} \Gamma_- \\ -\Gamma_+ \end{pmatrix} \frac{r_{\downarrow\uparrow}}{i\frac{R_0}{v_\mathrm{F}}\cos\theta\sin^3\theta}
$$
$$
= \begin{pmatrix} \Gamma_+(2\gamma_0 d) + r_{\uparrow\uparrow}\Gamma_-(2\gamma_0 d) \\ -\Gamma_-(2\gamma_0 d) + r_{\uparrow\uparrow}\Gamma_+(2\gamma_0 d) \end{pmatrix} + \mathcal{O}(\epsilon^2) \tag{B24}
$$

It follows from Eq. (B24)

$$
r_{\uparrow\uparrow} = -\frac{\cos(2\theta) + i[\mathrm{sh}(2\gamma_0 d) - \sin(2\theta)\mathrm{ch}(2\gamma_0 d)]}{\mathrm{ch}(2\gamma_0 d) - \sin(2\theta)\mathrm{sh}(2\gamma_0 d)} + \mathcal{O}(\epsilon^2) \ , \tag{B25}
$$

and

$$
r_{\downarrow\uparrow} = \frac{\epsilon}{2} \frac{\sin(2\theta)[1 - \cos(2\theta)]}{\mathrm{ch}(2\gamma_0 d) - \sin(2\theta)\mathrm{sh}(2\gamma_0 d)} + \mathcal{O}(\epsilon^2) \ . \tag{B26}
$$

3. An electron incident from the spin-down channel

The reflection amplitudes for an electron incident from the spin-down channel can be solved similarly. Now the wavefunction in the electrode is given by

$$
\Psi_E(x) = \frac{1}{\sqrt{2}}|\downarrow\rangle \otimes \begin{pmatrix} 1 \\ 1 \end{pmatrix} + \frac{r_{\downarrow\downarrow}}{\sqrt{2}}|\downarrow\rangle \otimes \begin{pmatrix} 1 \\ -1 \end{pmatrix} + \frac{r_{\uparrow\downarrow}}{\sqrt{2}}|\uparrow\rangle \otimes \begin{pmatrix} 1 \\ 1 \end{pmatrix} \ . \tag{B27}
$$

The forms of the wavefunctions in the pump and barrier remain to be the same. By some algebra, we arrive at

$$
\Psi_B(0^+) = \frac{1}{\sqrt{2}} \begin{pmatrix} r_{\uparrow\downarrow}\Gamma_-(2\gamma_0 d) \\ r_{\uparrow\downarrow}\Gamma_+(2\gamma_0 d) \\ \Gamma_+(2\gamma_0 d) + r_{\downarrow\downarrow}\Gamma_-(2\gamma_0 d) \\ \Gamma_-(2\gamma_0 d) - r_{\downarrow\downarrow}\Gamma_+(2\gamma_0 d) \end{pmatrix} \ . \tag{B28}
$$

Equating Eq. (B14) with Eq. (B28), we obtain

$$
\begin{pmatrix} -i\cos^2\theta & \sin\theta\cos\theta \\ -\sin\theta\cos\theta & -i\sin^2\theta \end{pmatrix} \begin{pmatrix} \Gamma_- \\ -\Gamma_+ \end{pmatrix} \frac{r_{\uparrow\downarrow}}{i\frac{R_0}{v_\mathrm{F}}\cos^3\theta\sin\theta}
$$
$$
= \begin{pmatrix} \Gamma_+(2\gamma_0 d) + r_{\downarrow\downarrow}\Gamma_-(2\gamma_0 d) \\ \Gamma_-(2\gamma_0 d) - r_{\downarrow\downarrow}\Gamma_+(2\gamma_0 d) \end{pmatrix} + \mathcal{O}(\epsilon^2) \tag{B29}
$$

It follows from Eq. (B29)

$$
r_{\downarrow\downarrow} = \frac{\cos(2\theta) - i[\mathrm{sh}(2\gamma_0 d) - \sin(2\theta)\mathrm{ch}(2\gamma_0 d)]}{\mathrm{ch}(2\gamma_0 d) - \sin(2\theta)\mathrm{sh}(2\gamma_0 d)} + \mathcal{O}(\epsilon^2) \ , \tag{B30}
$$

and

$$
r_{\uparrow\downarrow} = -\frac{1}{2} \frac{\sin(2\theta)[1 + \cos(2\theta)]}{\mathrm{ch}(2\gamma_0 d) - \sin(2\theta)\mathrm{sh}(2\gamma_0 d)} \left(\frac{R_0}{v_\mathrm{F}}\right) + \mathcal{O}(\epsilon^2) \ . \tag{B31}
$$

4. A verification of the result

The total Hamiltonian of the system is invariant under the transformation

$$
(-i\hat{s}_y\hat{\sigma}_z)H(-\tilde{k}_y)(i\hat{s}_y\hat{\sigma}_z) = H(\tilde{k}_y) \ , \tag{B32}
$$

so the corresponding transformation of Eq. (B18)

$$(-i\hat{s}_y\hat{\sigma}_z) \quad \Psi_E(x)|_{\tilde{k}_y\to-\tilde{k}_y} = \frac{1}{\sqrt{2}}|\downarrow\rangle\otimes\begin{pmatrix}1\\1\end{pmatrix}$$

$$+\frac{r_{\uparrow\uparrow}|_{\tilde{k}_y\to-\tilde{k}_y}}{\sqrt{2}}|\downarrow\rangle\otimes\begin{pmatrix}1\\-1\end{pmatrix}$$

$$-\frac{r_{\downarrow\uparrow}|_{\tilde{k}_y\to-\tilde{k}_y}}{\sqrt{2}}|\uparrow\rangle\otimes\begin{pmatrix}1\\1\end{pmatrix} , \tag{B33}$$

must also be an eigenstate of $H(\tilde{k}_y)$. This result tells that an electron incident from the spin-down channel will be reflected into the spin-down channel with amplitude $r_{\uparrow\uparrow}|_{\tilde{k}_y\to-\tilde{k}_y}$, and also into the spin-up channel with amplitude $-r_{\downarrow\uparrow}|_{\tilde{k}_y\to-\tilde{k}_y}$. Comparing it with Eq. (B27) and noticing that $\tilde{k}_y \to -\tilde{k}_y$ is equivalent to $2\theta \to (\pi-2\theta)$, we find immediately the following relations

$$r_{\downarrow\downarrow} = r_{\uparrow\uparrow}|_{2\theta\to(\pi-2\theta)} , \tag{B34}$$

and

$$r_{\uparrow\downarrow} = -r_{\downarrow\uparrow}|_{2\theta\to(\pi-2\theta)} . \tag{B35}$$

The reflection amplitudes given in Eqs. (B25), (B26), (B30), and (B31) apparently satisfy these relations.

Appendix C: CALCULATION OF THE REFLECTION AMPLITUDES FOR A HALF-METALLIC ELECTRODE

To simulate the half-metallic electrode, the Hamiltonian of the electrode is taken to be $H_E = v_F'(k_y)k_x\hat{s}_z\hat{\sigma}_x + V_1(\hat{1}\mp\hat{s}_z)\hat{\sigma}_z/2$. Consider first the case, where the spin polarization of the electrode is parallel to the z-axis. Now the Hamiltonian of the potential barrier becomes

$$H_B = H_E + \begin{pmatrix}0 & 0\\0 & V_1\hat{\sigma}_z\end{pmatrix} . \tag{C1}$$

For simplicity, we will take $V_1 \to \infty$ limit in the final result. In this case, an electron incident from the spin-up channel has some probability to be reflected into the spin-down channel from the pump, but the reflected wave will decay quickly to 0 within the barrier, and has no chance to reach the electrode. Therefore, $r_{\downarrow\uparrow} \equiv 0$ and the wavefunction in the electrode becomes

$$\Psi_E(x) = \frac{1}{\sqrt{2}}|\uparrow\rangle\otimes\begin{pmatrix}1\\-1\end{pmatrix} + \frac{r_{\uparrow\uparrow}}{\sqrt{2}}|\uparrow\rangle\otimes\begin{pmatrix}1\\1\end{pmatrix} . \tag{C2}$$

The wavefunction in the potential barrier can be written as

$$\Psi_B(x) = \frac{C_1}{\sqrt{2}}|\uparrow\rangle\otimes\begin{pmatrix}1\\-i\end{pmatrix}e^{\gamma_0 x} + \frac{C_2}{\sqrt{2}}|\uparrow\rangle\otimes\begin{pmatrix}1\\i\end{pmatrix}e^{-\gamma_0 x} + \frac{C_3}{\sqrt{2}}|\downarrow\rangle\otimes\begin{pmatrix}1\\-i\end{pmatrix}e^{-\gamma_1 x} , \tag{C3}$$

where $\gamma_0 = V_0/\hbar v_F'$ and $\gamma_1 = V_1/\hbar v_F' \to \infty$. The wavefunction in the pump remains to be same. Repeating the same calculation as in sec. II, it is straightforward to obtain

$$r_{\uparrow\uparrow} = -\frac{\cos(2\theta) + i[\text{sh}(2\gamma_0 d) - \sin(2\theta)\text{ch}(2\gamma_0 d)]}{\text{ch}(2\gamma_0 d) - \sin(2\theta)\text{sh}(2\gamma_0 d)} + \mathcal{O}(\epsilon^2) . \tag{C4}$$

This expression is identical in form to Eq. (B25) obtained in Sec. II for a nonmagnetic electrode. However, an important difference is $r_{\downarrow\uparrow} \equiv 0$. As a result, $|r_{\uparrow\uparrow}|^2 \equiv (1-|r_{\downarrow\uparrow}|^2) \equiv 1$ up to any order in ϵ. This means that $\mathcal{O}(\epsilon^2)$ in Eq. (C4) must be a correction only to the argument of $r_{\uparrow\uparrow}$, which as discussed in the manuscript, will not modify the orbit of $r_{\uparrow\uparrow}$ on the complex plane. The orbit is always a unit circle for $|k_y| < k_y^c$, and the amount of charge pumped per cycle by the k_y state is quantized to $\Delta q(k_y) = -eC_+$. Similarly, for the spin polarization of the electrode antiparallel to the z-axis, the charge pumped per cycle is $\Delta q(k_y) = -eC_-$.

---

* Electronic address: shengli@nju.edu.cn

† Electronic address: dyxing@nju.edu.cn

1 K. Klitzing, G. Dorda, and M. Pepper, Phys. Rev. Lett. **45**, 494 (1980).

2 A. Tsukazaki, A. Ohtomo, T. Kita, Y. Ohno, H. Ohno, and M. Kawasaki, Science **315**, 1388 (2007).

3 Y. Zhang, Y. W. Tan, H. L. Stormer, and P. Kim, Nature **438**, 201-204 (2005).

4 C. Brüne, C. X. Liu, E. G. Novik, E. M. Hankiewicz, H. Buhmann, Y. L. Chen, X. L. Qi, Z. X. Shen, S. C. Zhang, and L. W. Molenkamp, Phys. Rev. Lett. **106** 126803 (2011).

5 R. B. Laughlin, Phys. Rev. B **23**, 5632 (1981).

6 D. J. Thouless, M. Kohmoto, M. P. Nightingale, and M. den Nijs, Phys. Rev. Lett. **49**, 405 (1982).

7 Q. Niu, and D. J. Thouless, J. Phys. A: Math. Gen. **17**, 2453 (1984).

8 D. J. Thouless, Phys. Rev. B **27**, 6083 (1983).

9 C. L. Kane, and E. J. Mele, Phys. Rev. Lett. **95**, 226801 (2005).

10 B. A. Bernevig,and S. C. Zhang, Phys. Rev. Lett. **96**, 106802 (2006).

11 M. König, S. Wiedmann, C. Brüne, A. Roth, H. Buhmann, L. W. Molenkamp, X. L. Qi, and S. C. Zhang, Science **318**, 766 (2007).

12 I. Knez and R. R. Du, Frontiers of Phys. **7**, 200 (2012).

13 J. E. Moore and L. Balents, Phys. Rev. B **75**, 121306 (R) (2007).

14 L. Fu and C. L. Kane, Phys. Rev. B **76**, 045302 (2007).

15 M. Z. Hasan, and C. L. Kane, Rev. Mod. Phys. **82**, 3045 (2010).

16 X. L. Qi and S. C. Zhang, Physics Today **63**, 33 (2010).

17 F. D. M. Haldane, Phys. Rev. Lett. **61**, 2015 (1988).

18 C. L. Kane and E. J. Mele, Phys. Rev. Lett. **95**, 146802 (2005).

19 D. N. Sheng, Z. Y. Weng, L. Sheng, and F. D. M. Haldane, Phys. Rev. Lett. **97**, 036808 (2006).

20 E. Prodan, Phys. Rev. B **80**, 125327 (2009).

21 Y. Yang, Z. Xu, L. Sheng, B. G. Wang, D. Y. Xing, and D. N. Sheng, Phys. Rev. Lett. **107**, 066602 (2011).

22 X. L. Qi, T. L. Hughes, and S. C. Zhang, Phys. Rev. B **78**, 195424 (2008).

23 A. M. Essin, J. E. Moore, and D. Vanderbilt, Phys. Rev. Lett. **102**, 146805 (2009).

24 L. Fu, and C. L. Kane, Phys. Rev. B **74**, 195312 (2006).

25 C. Q. Zhou, Y. F. Zhang, L. Sheng, R. Shen, D. N. Sheng, and D. Y. Xing, Phys. Rev. B **90**, 085133 (2014).

26 X. L. Qi, T. L. Hughes, and S. C. Zhang, Nature Physics **4**, 273 (2008).

27 F. Mahfouzi, B. K. Nikolić, S. H. Chen, and C. R. Chang, Phys. Rev. B **82**, 195440 (2010).

28 B. A. Bernevig, T. L. Hughes, and S. C. Zhang, Science **314**, 1757-1761 (2006).

29 M. König, H. Buhmann, L. W. Molenkamp, T. L. Hughes, C. X. Liu, X. L. Qi, and S. C. Zhang, J. Phys. Soc. Jpn. **77**, 031007 (2008).

30 W. Yang, K. Chang, and S. C. Zhang, Phys. Rev. Lett. **100**, 056602 (2008).

31 C. X. Liu, T. L. Hughes, X. L. Qi, K. Wang, and S. C. Zhang, Phys. Rev. Lett. **100**, 236601 (2008).

32 D. G. Rothe, R. W. Reinthaler, C. X. Liu, L. W. Molenkamp, S. C. Zhang, and E. M. Hankiewicz, New J. Phys. **12**, 065012 (2010).

33 G. H. Wannier, Rev. Mod. Phys. **34**, 645 (1962).

34 X. L. Qi, Phys. Rev. Lett. **107**, 126803 (2011).

35 H. Li, L. Sheng, and D. Y. Xing, Phys. Rev. Lett. **108**, 196806 (2013).

36 M. Büttiker, H. Thomas, and A. Prêtre, Z. Phys. B **94**, 133 (1994).

37 P. W. Brouwer, Phys. Rev. B **58**, R10135 (1998).

38 M. Switkes, C. M. Marcus, K. Campman, and A. C. Gossard, Science **283**, 1905 (1999).

39 F. Giazotto, P. Spathis, S. Roddaro, S. Biswas, F. Taddei, M. Governale, and L. Sorba, Nature Physics **7**, 857 (2011).

40 G. E. W. Bauer, and Y. Tserkovnyak, Physics **4**, 40 (2011).